Heliyon 10 (2024) e37151

Contents lists available at ScienceDirect

Heliyon

journal homepage: www.cell.com/heliyon

Research article

Cu immobilized on $MgZnFe_2O_4$ nanoparticles as a green catalyst in the synthesis of mono and bis-polyhydroquinolines

Zahra Abbas-Ordoo [a], Akbar Mobinikhaledi [a,b,*], Mohammad Ali Bodaghifard [a,b]

[a] Department of Chemistry, Faculty of Science, Arak University, Arak, 38481-77584, Iran
[b] Institute of Nanosciences and Nanotechnology, Arak University, Arak, Iran

ARTICLE INFO

Keywords:
Magnetic nanoparticles
Multicomponent reaction
Ziziphus spina-christi extract
Hantzsch reaction

ABSTRACT

In this study, a green and environmentally friendly catalyst ($MgZnFe_2O_4$@ZSC-Cu) was synthesized using a simple and clean method. The catalyst was prepared by combining $MgZnFe_2O_4$ MNPs with Ziziphus spina-christi extract (ZSC) and immobilizing Cu ions on the resulting material. The catalyst was thoroughly characterized using various techniques including Fourier-transform infrared spectroscopy (FT-IR), X-ray diffraction (XRD), Field emission-scanning electron microscopy (FE-SEM), Energy dispersive X-ray analyzer (EDS), Inductively coupled plasma-optical emission spectrometry (ICP-OES), Thermogravimetric (TGA), and Vibrating sample magnetometry (VSM) analyses. The catalytic activity of $MgZnFe_2O_4$@ZSC-Cu was evaluated in the Hantzsch reaction involving a four-component reaction with ethyl acetoacetate or dimedone/cyclohexane-1,3-dione, various aromatic aldehydes/di-aldehydes, and ammonium acetate. The structure of the newly formed bis compound and polyhydroquinolines was determined using FT-IR, ^1H and ^{13}C NMR spectroscopy. This catalyst provides numerous benefits, such as simple separation using a magnet, less reaction times, high product yield, solvent-free conditions, straightforward work-up, and the capability to reuse the catalyst for up to five cycles.

1. Introduction

Magnetic nanoparticles (MNPs) are a crucial class of nanomaterials with a wide range of practical applications including ferrofluids [1], biosensors [2], catalysts [3], drug delivery systems [4], cell therapy [5], imaging techniques [6], antibacterial agents and cytotoxicity studies [7], and etc. The biocompatibility, the ability to be easily separated using an external magnetic field, and high stability are among the key advantages of these compounds, which have contributed to their popularity in various industries [8–10]. There are many methods for the preparation of MNPs. Various methods utilized for the synthesis of nanoparticles, such as co-precipitation, microemulsion, sol-gel reactions, sonochemical synthesis, hydrothermal methods, thermal decomposition, decomposition of organometallic precursors, and polyol methods [11,12]. Although there are numerous synthetic methods available for producing MNPs, it remains crucial to identify cost-effective, and eco-friendly approaches for their preparation. The selection of the synthesis method will be determined by the specific properties desired for the magnetic nanoparticles, the equipment availability and cost, as well as its ability to be scalable. Type of plants contain phytochemicals like phenolic compounds, heterocyclic compounds, alkaloids, terpenoids, and flavonoids were successfully applicated to prepare nanoparticles of various metal oxides or metals [13]. The biosynthetic reaction

* Corresponding author. Department of Chemistry, Faculty of Science, Arak University, Arak, 38481-77584, Iran.
E-mail address: akbar_mobini@yahoo.com (A. Mobinikhaledi).

https://doi.org/10.1016/j.heliyon.2024.e37151
Received 3 June 2024; Received in revised form 25 August 2024; Accepted 28 August 2024
Available online 4 September 2024

plays a crucial role in determining the size and shape of nanoparticles. Various factors, including the type of plant extract, the season, the location of the plant organ, and metal salt concentration, can influence the final outcome of the nanoparticles produced. The process of synthesizing MNPs with plant parts has an effect on the physical, chemical, and biological behavior. Microorganism-mediated green route techniques and plant extracts have played a crucial role in reducing ferrite particle aggregation. This is achieved through the presence of phenolics, natural proteins, and other contents that act as stabilizers and coat the prepared nanoparticles, which effectively prevent the particles from clumping together, resulting in improved stability and dispersion of the nanoparticles. MNPs produced by plant extract can be transformed into nanoparticles via redox reactions by various phytoconstituents [14].

Several examples of green synthesis of nanoparticles using plant extracts include the synthesis of silver nanoparticles from dried bark extract of Catharanthus roseus deposited on graphene oxide (AgNPs/GO) [15], copper nanoparticles using a hydroalcoholic extract of Moringa oleifera Leaves (Cu NPs) [16], magnetic Fe_3O_4 nanoparticles using Couroupita guianensis Aubl. fruit extract [7]. Utilizing plant extracts in the synthesis of nanoparticles offers numerous benefits, including their widespread availability, rapid synthesis process, and ease of scaling-up. The plant extracts contain a combination of biomolecules that aid in the reduction of metals and formation of material nanoparticles. As a result, the utilization of plant extracts for the preparation of metal nanoparticles is on the rise [13,17].

Ziziphus spina-christi (ZSC) is a plant belonging to the Rhamnaceae family within the order of Rosales. This plant is part of a diverse group that includes approximately 60 genera and over 850 species. ZSC (sedr) has played a significant role in Iranian traditional medicine for centuries and can be found growing naturally throughout Iran. ZSC is rich in various compounds, including Geranyl acetate, methyl octadecanoate, methyl hexadecanoate, hexadecanol, ethyl octadecanoate, farnesyl acetone C, jubanine-A, amphibine-H, Zizyphine-F, and spinanine-A [18]. ZSC has been shown various biological activities, including antibacterial, antifungal, antioxidant, antidiabetic, analgesic, antinociceptive, antiplasmodial, antischistosomiasis, and anticonvulsant properties [18–20]. Due to the biological activities, cheapness, and availability of ZSC extract, in this paper, ZSC extract as a precursor to prepare $MgZnFe_2O_4$@ZSC MNPs.

One of the most significant applications of MNPs is their catalytic role in multi-component reactions [21–23]. These reactions provide a multitude of benefits, such as increased efficiency, minimized by-products, gentle operating conditions, rapid reaction times, and high selectivity [24,25]. Polyhydroquinolines are a class of heterocycles with significant pharmaceutical potential, including calcium antagonists for treating coronary heart disease [26], antimicrobial properties [26], antioxidant effects [27], anti-inflammatory [26], and etc. These compounds are vital for biological researches due to their diverse activities. The synthesis of polyhydroquinolines has been achieved using various catalysts such as FeF_3 [28], Ni-Cu-$MgFe_2O_4$ [29], Fe_3O_4@D-NH-$(CH_2)_4$-SO_3H [30], Fe_3O_4@TiO_2--Pr-2AB@Cu [31] and MNPs–BSAT [7]. Several methods have been reported for the synthesis of polyhydroquinolines. However, some of these methods suffer from drawbacks such as challenging and time-consuming purification steps, difficulties in catalyst separation, and the use of catalysts that require lengthy manufacturing processes. Due to the significant role of polyhydroquinolines in various biological applications, it is imperative to explore innovative and eco-friendly approaches utilizing green catalysts for their synthesis.

Following our researches on the synthesis of nitrogen-containing heterocycles [7,32,33], here, an environmentally friendly method is presented for preparation of polyhydroquinolines. This innovative procedure utilizes a copper complex stabilized on $MgZnFe_2O_4$@ZSC particles as a magnetically separable catalyst, making it efficient and sustainable.

2. Experimental

2.1. Measurements

The characterization techniques employed in the present study are introduced. FT-IR spectra was reported via a Jasco-680 spectrophotometer (Japan) at room temperature in the wave number to identify functional groups. Surface morphological and elemental observation studies were done by the use of Field Emissive Scanning Electron Microscopy (FE-SEM, Philips FEI Quanta-200f) and Energy dispersive X-ray Analysis (EDAX, Oxford Instruments). The amounts of Cu leaching into solution for the catalyst was determined through ICP elemental analysis (analytikjena 9100). The crystalline structure of the samples was examined by X-ray powder diffractometric Bruker AX500 X-ray diffractometer under Cu-Kα radiation (0.154 nm) at room temperature. The magnetic properties of samples were testes by Vibrating Sample Magnetometer (VSM) (lakeshore-Model: 7404) at room temperature. ^{1}H NMR spectra were obtained with Bruker Avance spectrometer 300 MHz and ^{13}C NMR spectra were also reported with INOVA 500 MHz in DMSO-d_6 with TMS as an internal standard. Thermal gravimetric analysis (TGA and DTG) was conducted on a TA instruments Q 5000 system for characterizing thermal stability of the catalyst over a temperature limited area of 30–700 °C with a heating rate of 10 °C/min under nitrogen atmosphere.

3. Materials

All materials ($Zn(NO_3)_2.6H_2O$, $Mg(NO_3)_2.6H_2O$, $Fe(NO_3)_3.9H_2O$, $(Cu(CH_3COO)_2)$, ammonium hydroxide (NH_3, 28–30 % aqueous solution) were analytical grade procured from Merck Chemical Co. and used for producing purpose catalyst. Meanwhile, fresh leaves of Ziziphus spina-christi were collected from Dezful city, Iran.

3.1. Synthesis of MgZnFe2O4@ZSC-Cu nanoparticles

3.1.1. Preparation of plant extract

The Ziziphus spina-christi extract was prepared using ultrasonic waves, as described in a previous study [34]. Fresh leaves of Ziziphus spina-christi were carefully collected, washed with distilled water, dried, and grounded to prepare them for extraction. The grounded leaves were then placed into a 250 mL round flask and subjected to sonication with a mixture of 120 mL ethanol and 30 mL water at a temperature of 40 °C for a duration of 50 min. Afterward, the extract was cooled to room temperature and filtered using Whatman filter paper No. 1 to eliminate any solid particles.

3.1.2. Synthesis of $MgZnFe_2O_4$@ZSC nanoparticles

The $MgZnFe_2O_4$@ZSC ferrite nanoparticles were synthesized using a previously established method [35]. In summary, Zn $(NO_3)_2.6H_2O$ (2.5 mmol, 0.74 g), $Mg(NO_3)_2.6H_2O$ (2.5 mmol, 0.64 g) and $Fe(NO_3)_3.9H_2O$ (10 mmol, 4.40 g) were combined in a solution containing 40 mL of water and 60 mL of Ziziphus spina-christi extract as a surfactant. The mixture was stirred until homogeneous and then subjected to reflux. Ammonia (NH_3, 30 %) was introduced as a precipitating agent and the reaction proceed under specified conditions. The resulting sediment was washed with water (250 mL) six times and ethanol (25 mL) three times. Finally, the sediment was dried in an oven at 70 °C and calcined at 600 °C to yield the final nanoparticles.

3.1.3. Synthesis of $MgZnFe_2O_4$@ZSC-Cu nanoparticles

The Cu ions were coated on $MgZnFe_2O_4$@ZSC NPs by an easy method. 1 g of $MgZnFe_2O_4$@ZSC NPs was sonicated in ethanol (99 %) for 30 min. Separately, $Cu(CH_3COO)_2$ (2 mmol, 0.36 g) was added to the mixture and stirred under N_2 atmosphere for 24 h. The brown magnetic nanoparticles were separated using a magnet, washed with ethanol, dried, and powdered to obtain the ferrite nanoparticles (FNPs).

3.1.4. General procedure for preparation of mono-polyhydroquinolines

A mixture of aldehyde (**1**, 1 mmol), cyclic diketone (**2** or **3**, 1 mmol), ethylacetoacetate (**4**, 1 mmol, 0.13 mL), ammonium acetate (**5**, 1.5 mmol, 0.12 g) and the nanocatalyst (8 mg) was added to a test tube and stirred at 100 °C for relevant time (Table 1). The mixture was cooled to room temperature, dissolved in ethanol, and the magnetic nanoparticle (MNP) was separated using an external magnet. The solution was then concentrated and poured into water. The resulting precipitate was observed, filtered, and purified through recrystallization in ethanol to give 1,4-dihydroquinoline derivatives, which were then air-dried.

3.1.5. General procedure for preparation of bis-polyhydroquinolines

A mixture containing aldehyde (**1**, 1 mmol), cyclic diketone (**2** or **3**, 2 mmol), ethylacetoacetate (**4**, 2 mmol, 0.26 g), ammonium acetate (**5**, 3 mmol, 0.24 g), and a nanocatalyst (8 mg) was combined in a test tube and stirred at 100 °C for a specific duration. The progress of reaction was monitored using TLC. After completion of the reaction, the mixture was cooled to room temperature. It was then dissolved in ethanol, and the magnetic nanoparticles (MNP) were separated using an external magnet. The solution was then concentrated and poured into water. The resulting precipitate was filtered, and purified through recrystallization in ethanol to offer high yields of 1,4-dihydroquinoline derivatives, which were subsequently air-dried. The new compounds were characterized by ^{1}H-NMR and ^{13}C NMR spectroscopies.

Table 1
Optimal reaction conditions for the synthesis of 5a.

Entry	Catalyst (mg)	Solvent	Temperature (°C)	Time (min)	Yield[a] (%)
1	$MgZnFe_2O_4$@ZSC-Cu (20)	THF	Reflux	88	68
2	$MgZnFe_2O_4$@ZSC-Cu (20)	DMF	Reflux	51	78
4	$MgZnFe_2O_4$@ZSC-Cu (20)	MeOH	Reflux	30	75
5	$MgZnFe_2O_4$@ZSC-Cu (20)	Acetonitrile	Reflux	48	76
6	$MgZnFe_2O_4$@ZSC-Cu (20)	Acetone	Reflux	110	42
7	$MgZnFe_2O_4$@ZSC-Cu (20)	EtOH	Reflux	38	95
8	$MgZnFe_2O_4$@ZSC-Cu (20)	Chloroform	Reflux	160	40
9	$MgZnFe_2O_4$@ZSC-Cu (20)	H_2O	100	29	84
10	$MgZnFe_2O_4$@ZSC-Cu (20)	EtOH/H_2O	Reflux	35	94
11	$MgZnFe_2O_4$@ZSC-Cu (20)	Solvent free	100	10	93
12	$MgZnFe_2O_4$@ZSC-Cu (10)	Solvent free	100	6	94
13	$MgZnFe_2O_4$@ZSC-Cu (8)	Solvent free	100	4	96
14	$MgZnFe_2O_4$@ZSC-Cu (6)	Solvent free	100	15	90
15	$MgZnFe_2O_4$@ZSC-Cu (8)	Solvent free	80	20	91
16	$MgZnFe_2O_4$@ZSC-Cu (8)	Solvent free	60	28	80
17	_	Solvent free	100	160	trace
18	$MgZnFe_2O_4$@ZSC (8)	Solvent free	100	56	75

[a] obtaned yeild. Condition: benzaldehyde (1 mmol, 0.11 mL), dimedone (1 mmol, 0.14 g), ethyl acetoacetate (1 mmol, 0.13 mL), ammonium acetate (1.5 mmol, 0.12 g).

3.2. Selected data

3.2.1. Ethyl 2,7,7-trimethyl-5-oxo-4-phenyl-1,4,5,6,7,8-hexahydroquinoline-3 carboxylate (5a)

IR (KBr, cm^{-1}): ν_{max} = 3288, 3216, 3080, 2960, 2933, 1699, 1644, 1601, 1485, 1382, 1280, 1214. ^{1}H NMR (300 MHz, DMSO-d_6): δ_H = 0.81 (s, 3H, CH_3), 0.98 (s, 3H, CH_3), 1.10 (t, 3H, J = 7.0 Hz, CH_3), 1.97–2.48 (m, 4H, CH_2), 2.25 (s, 3H, CH_3), 3.94 (q, 2H, J= 7.0 Hz, CH_2), 4.81 (s, 1H, CH), 7.01–7.18 (m, 5H, H_{Ar}), 9.06 (s, 1H, NH) ppm. ^{13}C NMR (75 MHz, DMSO-d_6): 14.5, 18.8, 26.8, 29.5, 32.6, 36.5, 50.6, 59.6, 103.4, 109.9, 113.5, 126.9, 128.8, 130.5, 146.0, 150.3, 167.0, 194.7 [36]. Anal. Calcd for $C_{21}H_{25}NO_3$: C, 74.31; H, 7.42; N, 4.13 %. Found: C, 74.52; H, 7.11; N, 3.9 %.

3.2.2. Ethyl 4-(4-fluorophenyl)-2,7,7-trimethyl-5-oxo-1,4,5,6,7,8-hexahydroquinoline-3-carboxylate (5b)

IR (KBr, cm^{-1}): ν_{max} = 3276, 3204, 3077, 2962, 2934, 1707, 1646, 1605, 1382, 1280, 1217, 854. ^{1}H NMR (300 MHz, DMSO-d_6): δ_H = 0.86 (s, 3H, CH_3), 1.00 (s, 3H, CH_3), 1.14 (t, 3H, J = 7.0 Hz, CH_3), 1.94–2.44 (m, 4H, CH_2), 2.25 (s, 3H, CH_3), 3.98 (q, 2H, J = 7.0 Hz, CH_2), 4.77 (s, 1H, CH), 6.58–6.76 (m, 4H, H_{Ar}), 9.02 (s, 1H, NH) ppm. ^{13}C NMR (100 MHz, DMSO-d_6): 14.28, 19.40, 27.14, 29.51, 32.76, 36.14, 41.01, 50.79, 59.95, 106.04, 112.03, 114.63, 129.47, 143.04, 143.73, 148.62, 161.32, 167.45, 195.79 [37]. Anal. Calcd for $C_{21}H_{24}$ FNO_3: C, 70.57; H, 6.77; F, 5.32; N, 3.92 %. Found: C, 70.74; H, 6.56; F, 5.02; N, 3.75 %.

3.2.3. Ethyl 4-(3,4-dimethoxyphenyl)-2,7,7-trimethyl-5-oxo-1,4,5,6,7,8-hexahydroquinoline-3-carboxylate (5c)

IR (KBr, cm^{-1}): ν_{max} = 3278, 3211, 3078, 2938, 1695, 1603, 1513, 1489, 1271, 1216. ^{1}H NMR (300 MHz, DMSO-d_6): δ_H = 0.86 (s, 3H, CH_3), 1.00 (s, 3H, CH_3), 1.14 (t, 3H, J = 7.2 Hz, CH_3), 1.94–2.38 (m, 4H, CH_2), 2.25 (s, 3H, CH_3), 3.63 (s, 3H, -OCH_3) 3.65 (s, 3H, -OCH_3), 3.98 (q, 2H, J = 7.0 Hz, CH_2), 4.77 (s, 1H, CH), 6.58–6.76 (m, 3H, H_{Ar}), 9.02 (s, 1H, NH) ppm. ^{13}C NMR (100 MHz, DMSO-d_6): 18.2, 26.4, 29.2, 32.1, 34.9, 50.2, 50.6, 55.3, 55.4, 103.4, 110.0, 111.6, 118.9, 140.2, 144.8, 146.9, 148.01, 149.3, 167.3, 194.3 [38]. Anal. Calcd for $C_{23}H_{29}$ NO_5: C, 69.15; H, 7.32; N, 3.51 %. Found: C, 69.45; H, 7.03; N, 3.75 %.

3.2.4. Ethyl 4-(2,6-dichlorophenyl)-2,7,7-trimethyl-5-oxo-1,4,5,6,7,8-hexahydroquinoline-3-carboxylate (5d)

IR (KBr, cm^{-1}): ν_{max} = 3287, 3213, 3079, 2965, 2876, 1702, 1651, 1601, 1493, 1430, 1383, 1221. ^{1}H NMR (300 MHz, DMSO-d_6): δ_H = 0.87 (s, 3H, CH_3), 0.93 (s, 3H, CH_3), 1.03 (t, J = 7.0Hz, 3H, CH_3), 1.85 (d, J = 16.0 Hz, 1H, CH), 2.06–2.18 (m, 5H, CH_3 and CH_2), 2.34 (d, J = 16.0 Hz, 1H, CH), 3.85 (q, J = 7.0Hz, 2H, CH_2), 5.62 (s, 1H, CH), 7.04–7.28 (m, 3H, H_{Ar}), 9.10 (s, 1H, NH) ppm. ^{13}C NMR (100 MHz, DMSO-d_6): 14.07, 18.76, 27.42, 29.12, 31.90, 31.92, 35.53, 50.76, 59.16, 101.34, 108.07, 108.10, 126.81, 139.56, 146.20, 151.12, 167.46, 195.16 [37]. Anal. Calcd for $C_{21}H_{23}Cl_2$ NO_3: C, 61.77; H, 5.68; Cl, 17.36; N, 3.43 %. Found: C, 61.90; H, 5.48; Cl, 17.16; N, 3.70 %.

3.2.5. Ethyl 2-methyl-4-(4-nitrophenyl)-5-oxo-1,4,5,6,7,8-hexahydroquinoline-3-carboxylate (5e)

IR (KBr, cm^{-1}): ν_{max} = 3294, 3212, 3076, 2944, 1696, 1608, 1518, 1484, 1344, 1225. ^{1}H NMR (300 MHz, DMSO-d_6): δ_H = 1.10 (t, J = 12.0 Hz, 3H, CH_3), 1.71–2.29 (m, 9H, CH_3 and CH_2), 3.94 (q, J = 12.0 Hz, 2H, CH_2), 4.97 (s, 1H, CH), 7.38 (d, J = 8.0 Hz, 2H, H_{Ar}), 8.06 (d, J = 8.0 Hz, 2H, H_{Ar}), 9.31 (s, 1H, NH) ppm. ^{13}C NMR (100 MHz, DMSO-d_6): 14.61, 18.83, 21.23, 26.64, 36.93, 37.08, 59.77, 102.83, 110.70, 123.75, 129.24, 146.18, 146.60, 152.54, 155.70, 166.98, 195.16 [37]. Anal. Calcd for $C_{19}H_{20}$ N_2O_5: C, 64.04; H, 5.66; N, 7.86 %. Found: C, 64.31; H, 5.36; N, 7.66 %.

3.2.6. Ethyl 4-(3-hydroxyphenyl)-2-methyl-5-oxo-1,4,5,6,7,8-hexahydroquinoline-3-carboxylate (5f)

IR (KBr, cm^{-1}): ν_{max} = 3410, 3287, 3207, 3072, 2988, 1674, 1612, 1481, 1430, 1385, 1224. ^{1}H NMR (300 MHz, DMSO-d_6): 1.11 (t, J = 7.0 Hz, 3H, CH_3), 1.87 (d, J = 5 Hz, 1H, CH), 2.17 (t, 2H, J = 5.0 Hz, CH_2), 2.24 (s, 3H, CH_3), 2.43 (d, J = 5.0 Hz, 3H, CH_2 and CH), 3.96 (q, 2H, J = 7.0 Hz, CH_2), 4.80 (s, 1H, CH), 6.42–6.56 (m, 3H, H_{Ar}), 6.92 (t, J = 8.0 Hz, 1H, H_{Ar}), 9.09 and 9.10 (s, 2H, NH and OH) ppm. ^{13}C NMR (126 MHz, DMSO-d_6): 198.00, 167.74, 158.40, 155.56, 152.99, 145.76, 136.98, 130.17, 129.09, 120.10, 111.23, 103.30, 59.90, 35.08, 30.13, 27.30, 20.59, 18.97, 14.91. Anal. Calcd for $C_{19}H_{21}$ NO_4: C, 69.71; H, 6.47; N, 4.28 %. Found: C, 69.45; H, 6.70; N, 4.38 %.

3.2.7. Ethyl 4-(5-bromo-2-hydroxyphenyl)-2-methyl-5-oxo-1,4,5,6,7,8-hexahydroquinoline-3-carboxylate (5g)

IR (KBr, cm^{-1}): ν_{max} = 3312, 3271, 3091, 2978, 1733, 1654, 1585, 1480, 1376, 1237, 818. ^{1}H NMR (300 MHz, DMSO-d_6): δ_H = 0.99 (t, 3H, J = 7.11 Hz, CH_3), 1.68–1.85 (m, 6H, CH_2), 2.31 (s, 3H, CH_3), 3.90 (q, J = 7.11 Hz, 2H, CH_2), 4.89 (s, 1H, CH), 6.89–7.22 (m, 3H, H_{Ar}), 9.43 (s, 1H, OH), 9.73 (s, 1H, NH) ppm. ^{13}C NMR (126 MHz, DMSO-d_6): δ: 197.40, 166.57, 157.99, 154.36, 153.39, 145.32, 136.58, 131.17, 129.86, 119.11, 110.68, 103.31, 59.21, 40.03, 36.09, 31.13, 26.30, 20.47, 18.07, 13.91 ppm. Anal. Calcd for $C_{19}H_{20}$ $BrNO_4$: C, 56.17; H, 4.96; Br, 19.67; N, 3.45 %. Found: C, 56.46; H, 5.06; Br, 19.37; N, 3.75 %.

3.2.8. Diethyl 4,4'-((butane-1,4-diylbis(oxy))bis(2,1-phenylene))bis(2,7,7-trimethyl-5-oxo-1,4,5,6,7,8-hexahydroquinoline-3-carboxylate) (6a)

IR (KBr, cm^{-1}): ν_{max} = 3295, 3215, 3079, 2956, 2872, 1694, 1609, 1491, 1382, 1219. ^{1}H NMR (300 MHz, DMSO-d_6): δ_H = 0.80 (s, 6H, CH_3), 0.95 (s, 6H, CH_3), 1.05 (t, J = 7.0 Hz, 6H, CH_3), 1.84–1.90 (m, 6H, CH), 2.08–2.22 (m, 10H, CH and CH_3), 2.33–2.40 (m, 2H, CH_2), 3.84–3.97 (m, 8H, 4CH_2), 5.04 (s, 1H, CH), 5.06 (s, 1H, CH), 6.73 (t, J = 8.0 Hz, 2H, H_{Ar}), 6.84 (d, J = 8.0 Hz, 2H, H_{Ar}), 7.02 (t, J = 8.0 Hz, 2H, H_{Ar}), 7.12 (d, J = 8.0 Hz, 2H, H_{Ar}), 8.85 (s, 1H, NH), 8.92 (s, 1H, NH) ppm. ^{13}C NMR (126 MHz, DMSO-d_6): δ:194.3, 194.1, 167.3, 156.9, 156.9, 150.0, 149.8, 144.3, 134.7, 131.5, 126.9, 119.3, 111.9, 111.8, 109.0, 108.9, 102.8, 67.5, 58.8, 50.4, 39.5, 33.9, 32.0, 29.4, 29.3, 26.4, 26.1, 26.0, 18.3, 18.2, 14.1 ppm. Anal. Calcd for $C_{46}H_{56}$ N_2O_8: C, 72.23; H, 7.38; N, 3.66 %. Found: C,

72.50; H, 7.20; N, 3.40 %.

3.2.9. Diethyl 4,4'-((butane-1,4-diylbis(oxy))bis(4,1-phenylene))bis(2,7,7-trimethyl-5-oxo-1,4,5,6,7,8-hexahydroquinoline-3-carboxylate) (6b)

IR (KBr, cm^{-1}): ν_{max} = 3279, 3209, 3134, 2957, 1698, 1623, 1607, 1501, 1382, 1219. ^{1}H NMR (300 MHz, DMSO-d_6): δ_H = 0.82 (s, 6H, CH_3), 0.97 (s, 6H, CH_3), 1.10 (t, 6H, J = 7.0 Hz, CH_3), 1.75–2.41 (m, 18H, CH_2, CH_3), 3.88–3.97 (m, 8H, 4CH_2), 4.75 (s, 2H, 2CH), 6.70 (d, J = 8.0 Hz, 4H, H_{Ar}), 7.00 (d, J = 8.0 Hz, 4H, H_{Ar}), 9.00 (s, 2H, 2NH) ppm. ^{13}C NMR (126 MHz, DMSO-d_6): δ: 194.3, 166.9, 156.7, 149.2, 144.6, 140.0, 128.4, 113.6, 110.2, 103.9, 66.9, 59.0, 50.3, 40.0, 39.5, 34.9, 32.1, 29.2, 26.5, 25.5, 18.3, 14.2 ppm. Anal. Calcd for $C_{46}H_{56}N_2O_8$: C, 72.23; H, 7.38; N, 3.66 %. Found: C, 72.51; H, 7.51; N, 3.45 %.

3.2.10. Diethyl 4,4'-((propane-1,3-diylbis(oxy))bis(4,1-phenylene))bis(2,7,7-trimethyl-5-oxo-1,4,5,6,7,8-hexahydroquinoline-3-carboxylate) (6c)

IR (KBr, cm^{-1}): ν_{max} = 3283, 3204, 3079, 2958, 2874, 2877, 1669, 1607, 1501, 1382, 1219. ^{1}H NMR (300 MHz, DMSO-d_6): δ_H = 0.81 (s, 6H, CH_3), 0.97 (s, 6H, CH_3), 1.10 (t, 6H, J = 7.0 Hz, CH_3), 1.90–2.35 (m, 16H, CH_2, and CH_3), 3.90–4.00 (m, 8H, 4CH_2), 4.75 (s, 2H, 2CH), 6.72 (d, J = 8.0 Hz, 4H, H_{Ar}), 7.01 (d, J = 8.0 Hz, 4H, H_{Ar}), 9.00 (s, 2H, 2NH) ppm. ^{13}C NMR (126 MHz, DMSO-d_6): 194.3, 166.9, 156.5, 149.2, 144.7, 140.1, 128.4, 113.6, 110.2, 103.9, 64.0, 59.0, 50.3, 40.0, 39.5, 34.9, 32.1, 29.1, 28.8, 26.5, 18.3, 14.2 ppm. Anal. Calcd for $C_{45}H_{54}N_2O_8$: C, 71.98; H, 7.25; N, 3.73 %. Found: C, 71.78; H, 7.05; N, 3.94 %.

3.2.11. Diethyl 4,4'-(1,4-phenylene)bis(2-methyl-5-oxo-1,4,5,6,7,8-hexahydroquinoline-3-carboxylate) (6d)

IR (KBr, cm^{-1}): ν_{max} = 3286, 3215, 3078, 2948, 1692, 1609, 1480, 1379, 1224. ^{1}H NMR (300 MHz, DMSO-d_6): δ_H = 1.08 (q, J = 7Hz, 6H, 2CH_3), 1.73–2.28 (m, 18H, CH_2 and CH_3), 3.91–3.99 (m, 4H, 2CH_2), 4.79 (s, 2H, 2CH), 6.91 (s, 4H, H_{Ar}), 9.09 (s, 2H, 2NH) ppm. ^{13}C NMR (75 MHz, DMSO-d_6): δ: 194.7, 167.0, 151.6, 144.7, 141.4, 126.8, 110.9, 103.7, 59.0, 36.7, 36.7, 34.8, 26.1, 20.7, 18.3, 14.1 ppm. Anal. Calcd for $C_{32}H_{36}N_2O_6$: C, 70.57; H, 6.66; N, 5.14 %. Found: C, 70.69; H, 6.51; N, 5.43 %.

3.2.12. Diethyl4,4'-((propane-1,3-diylbis(oxy))bis(3-nitro-4,1-phenylene))bis(2-methyl-5-oxo-1,4,5,6,7,8-hexahydroquinoline-3-carboxylate) (6e)

IR (KBr, cm^{-1}): ν_{max} = 3294, 3216, 3080, 2947, 2897, 1693, 1641, 1615, 1528, 1486, 1377, 1226. ^{1}H NMR (300 MHz, DMSO-d_6): δ_H = 1.08 (s, 6H, 2CH_3), 1.71–2.27 (m, 20H, CH_2 and CH_3), 3.93 (s, 2H, CH_2), 4.19 (s, 6H, 3CH_2), 4.84 (s, 2H, 2CH), 7.19 (d, J = 8.0 Hz, 2H, H_{Ar}), 7.36 (d, J = 8.0 Hz, 2H, H_{Ar}), 7.52 (s, 2H, H_{Ar}), 9.22 (s, 2H, 2NH) ppm. ^{13}C NMR (126 MHz, DMSO-d_6): δ: 194.8, 166.5, 151.7, 149.6, 145.7, 140.5, 138.5, 133.6, 123.7, 114.6, 110.5, 102.7, 99.5, 65.4, 59.2, 40.0, 36.6, 35.1, 28.1, 26.1, 20.8, 18.3, 14.3, 14.0 ppm. Anal. Calcd for $C_{41}H_{44}N_4O_{12}$: C, 62.75; H, 5.65; N, 7.14 %. Found: C, 62.55; H, 5.38; N, 7.32 %.

4. Results and discussion

The synthesis of magnesium zinc ferrite magnetic nanoparticles modified by Copper ($MgZnFe_2O_4$@ZSC-Cu NPs) was followed according to the procedure outlined in Scheme 1. Initially, $MgZnFe_2O_4$ MNPs were synthesized through co-precipitation, with Ziziphus spina-christi leaves extract serving as both the surfactant and linker [39]. Subsequently, copper was immobilized onto the catalyst to produce $MgZnFe_2O_4$@ZSC-Cu NPs.

4.1. Characterization of $MgZnFe_2O_4$@ZSC-Cu

The constraction of $MgZnFe_2O_4$@ZSC-Cu was identified by the IR, EDX, XRD, TGA, VSM, FE-SEM, and ICP/OES.

Fig. 1 exhibits FT-IR spectra of both $MgZnFe_2O_4$@ZSC (a) and $MgZnFe_2O_4$@ZSC-Cu (b) NPs in the range of 400–4000 cm^{-1}. In the $MgZnFe_2O_4$@ZSC spectrum, there are two important bands that confirm the synthetic spinel structure. The appeared strong band at 570 cm^{-1} is belong to Fe-O stretching vibration, while the band at 420 cm^{-1} is referred to Mg-O stretching vibration in tetrahedral and octahedral configurations, respectively [40]. A clear set of bands is appeared at 1360-1630 cm^{-1}, which can prove the presence of functional groups in Ziziphus spina-christi leaves extract which overlapped with bending vibrations of adsorbed water molecules [41, 42]. Furthermore, a broad absorption band at 3400 cm^{-1} correlates to stretching vibration of O-H bonds. Moreover, a small move of this band to 3383 cm^{-1} (b) confirms the covalent bonds formation between Cu and $MgZnFe_2O_4$@ZSC nanoparticles [43], as well as the fabrication of $MgZnFe_2O_4$@ZSC-Cu NPs. Also, the creation of two new bands at 1217 and 1156 cm^{-1} confirms the presence of Cu complexes [7,44].

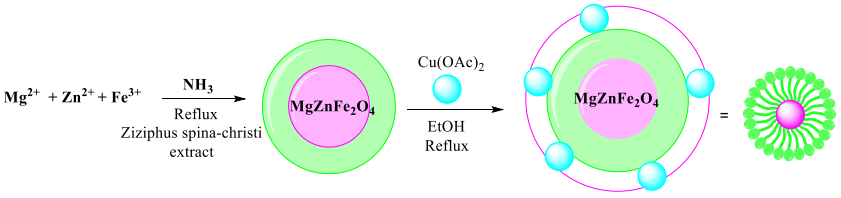

Scheme 1. The synthetic pathway of $MgZnFe_2O_4$@ZSC-Cu NPs.

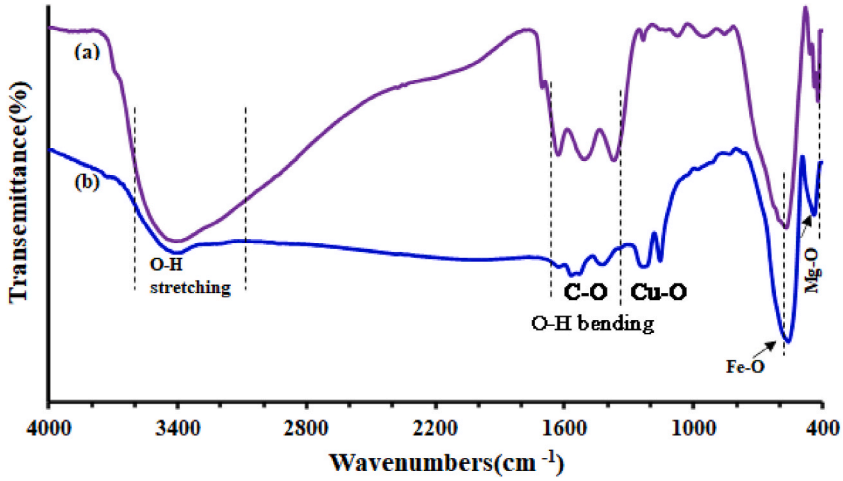

Fig. 1. FT-IR spectra of $MgZnFe_2O_4$ NPs (a), and $MgZnFe_2O_4$@ZSC-Cu NPs (b).

The X-ray powder diffraction (XRD) patterns of $MgZnFe_2O_4$@ZSC NPs (a) and MgZnFe2O4@ZSC-Cu NPs (b) are shown in Fig. 2. The XRD pattern indicates that the pure product is a single $MgZnFe_2O_4$ phase with a cubic spinel structure. All appeared peaks in pure MNPs patterns at $2\theta = 30°, 35°, 43°, 54°, 56.5°, 62.4°, 73.6°$ values, are corresponded to (220), (311), (222), (400), (422), (511), (440) planes, respectively, consistent with the patterns of $MgZnFe_2O_4$@ZSC NPs [43]. Compared to pure catalyst (a), $MgZnFe_2O_4$@ZSC-Cu NPs (b) exhibit the same patterns, confirming the structure. Additionally, three new peaks at 2θ values of 33°, 49°, 64° may belong to CuO NPs [45]. The crystallite size of $MgZnFe_2O_4$@ZSC-Cu NPs was calculated to be around 10 nm using the Debye-Scherrer equation from the XRD results, which is smaller than that obtained in SEM analysis. This difference may be due to the fact that XRD measurements typically consider crystallite sizes as the coherently diffracting domains of the material being studied. It is possible that grains or subgrains within the $MgZnFe_2O_4$@ZSC-Cu NPs contain various domains or regions with different crystallographic orientations, leading to discrepancies in the measured crystallite sizes.

Field emission scanning electron microscopy (FE-SEM) images were utilized to analyze the size and surface morphology $MgZnFe_2O_4$@ZSC-Cu nanoparticles (NPs) as shown in Fig. 3a. The mean diameter of the magnetic nanoparticles was determined to be 24 nm, with no visible agglomeration. This size is notably smaller compared to previous studies, likely attributed to the use of Ziziphus spina-christi leaves extract as a surfactant [39]. Qualitative energy-dispersive X-ray (EDX) analysis was conducted to assess the elemental composition of $MgZnFe_2O_4$@ZSC-Cu NPs. The EDX spectrum and elemental mapping of the synthesized NPs are depicted in Fig. 3b. The presence of Fe, Mg, Zn, O, C, and Cu elements was clearly identified, confirming the successful modification of $MgZnFe_2O_4$@ZSC NPs with copper. The amount of copper incorporated onto the $MgZnFe_2O_4$@ZSC NPs was quantified as 0.8 mmol/g using inductively coupled plasma optical emission spectrometry (ICP-OES).

The thermal stability of the NPs was evaluated using thermal analysis (TGA). The TGA and derivative thermogravimetric (DTG) diagram of the new catalyst were analyzed in a temperature range of 25–700 °C under N_2 atmosphere, as shown in Fig. 4. The thermogravimetric analysis (TGA) curve shows two clear weight losses. The first weight loss happens at low temperatures ($T < 100$ °C)

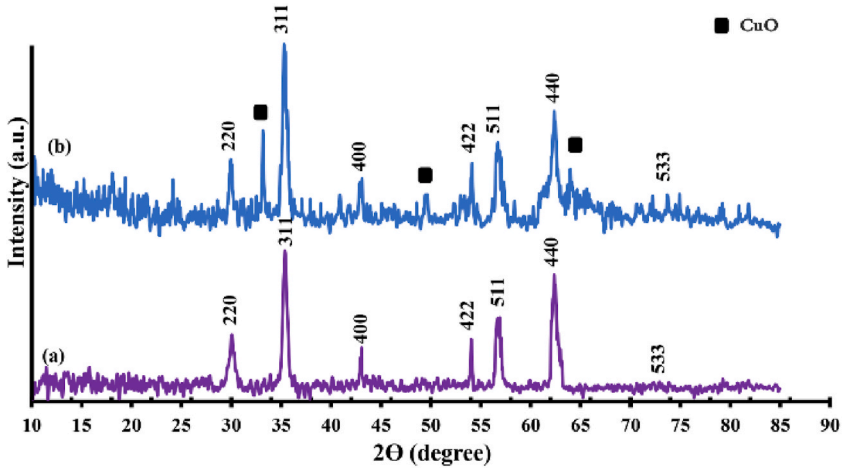

Fig. 2. XRD pattern of $MgZnFe_2O_4$ NPs (a), and $MgZnFe_2O_4$@ZSC-Cu NPs (b).

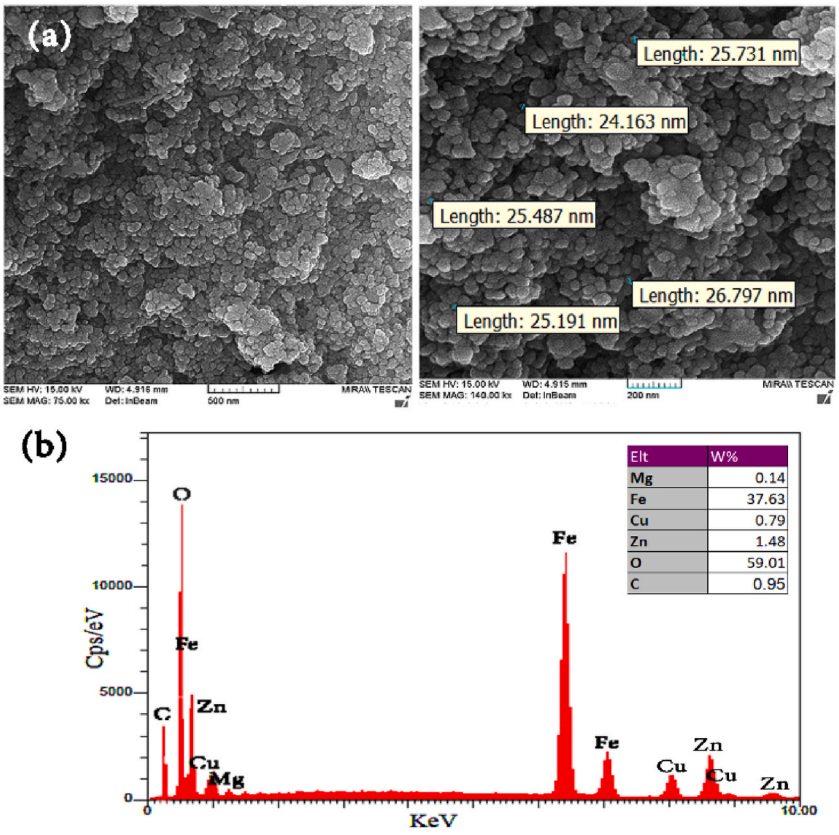

Fig. 3. FE-SEM image of $MgZnFe_2O_4$ NPs (a), and EDX spectra of $MgZnFe_2O_4$ NPs (b).

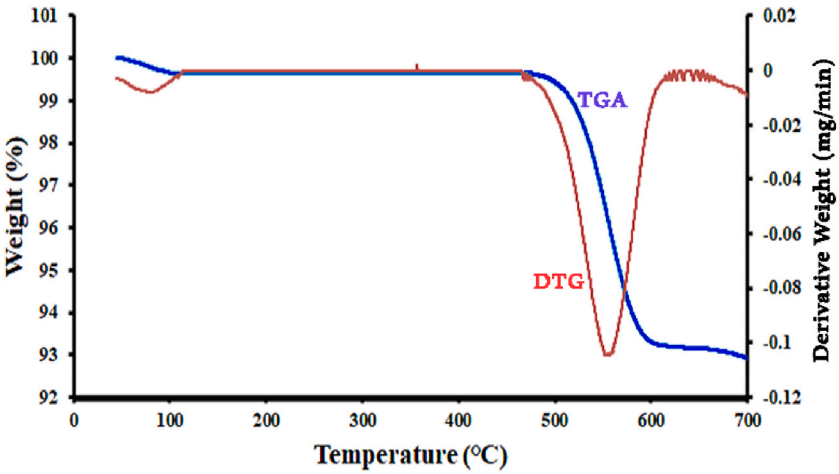

Fig. 4. TGA and DTG curves of $MgZnFe_2O_4$@ZSC-Cu NPs.

and is caused by the removal of adsorbed water, organic solvent, and surface hydroxyl groups from the $MgZnFe_2O_4$@ZSC-Cu nanoparticles. The second weight loss, approximately 7 %, occurs within the temperature range of 470–600 °C. This loss is attributed to a structural change in the MNPs, with no preceding alterations noted. Furthermore, the DTG analysis indicates the primary weight loss at 560 °C, corresponding to the structural change in the MNPs. Overall, the synthetic MNPs exhibit thermal stability up to 560 °C, suggesting that both copper and the extract are thermally stable and suitable for various applications.

The magnetic properties of $MgZnFe_2O_4$@ZSC nanoparticles (NPs) and $MgZnFe_2O_4$@ZSC-Cu NPs were analyzed using a Vibrating Sample Magnetometer (VSM) at room temperature, within a magnetic field range of ±9 kOe, as illustrated in Fig. 5. The results

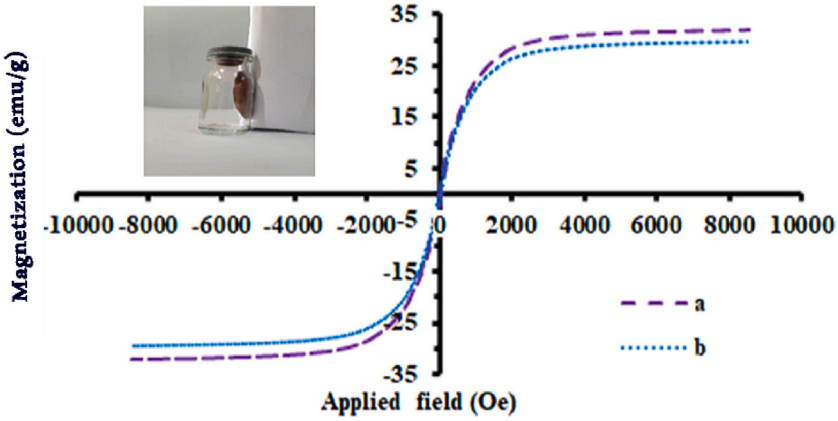

Fig. 5. Magnetization curve of $MgZnFe_2O_4$ NPs and $MgZnFe_2O_4$@ZSC-Cu NPs.

indicate a direct relationship between magnetization and increasing magnetic field, with no observed hysteresis in the magnetization of the two nanoparticles under examination. The saturation magnetization values were found to be 32 emu/g for $MgZnFe_2O_4$@ZSC NPs (a) and 30 emu/g for $MgZnFe_2O_4$@ZSC-Cu NPs (b). The decrease in saturation magnetization observed in $MgZnFe_2O_4$@ZSC-Cu NPs compared to $MgZnFe_2O_4$@ZSC NPs can be correlated to the presence of copper on the surface of the magnetic nanoparticles. Although there has been a slight decrease in magnetization, utilizing extracts to create $MgZnFe_2O_4$@ZSC-Cu nanoparticles with desirable magnetic properties is considered a valuable endeavor [46].

4.2. The synthesis of polyhydroquinoline derivatives via $MgZnFe_2O_4$@ZSC-Cu NPs as catalyst

The activity of this catalyst was studied through the Hantzsch reaction for synthesis of **5a** as a typical reaction. The reaction mixture is involved benzaldehyde (**1**, 1 mmol, 0.11 mL), dimedone (**2**, 1 mmol, 0.14 g), ethyl acetoacetate (**3**, 1 mmol, 13 mL), and ammonium acetate (**4**, 1.5 mmol, 0.12 g) (Scheme 2). The effect of solvent, temperature, amount of catalyst, and different catalysts was examined in this reaction. To determine the solvent effect and optimize the effective factors of desired reaction, various polar and non-polar solvents were chosen as the reaction medium, as shown in Table 1. While some solvents resulted in slow reactions, greener solvents like ethanol and water/ethanol mixture accelerated the reaction. The favorable results were obtained using 8 mg of the catalyst under solvent-free environment. In addition, the reaction rate was significantly improved by increasing the temperature up to 100 °C. The results suggest that temperature has a crucial role in enhancing the activity of the catalyst. Increasing the amount of catalyst to 8 mg led to the improvement in its activity. No increase in efficiency was observed up to 8 mg. The optimal amount of catalyst was found to be 8 mg. The effectiveness of 8 mg of $MgZnFe_2O_4$@ZSC-Cu NPs at 100 °C under solvent-free environment, which was determined to be the most favorable condition due to its high yield in this one-pot reaction (Table 1, Entry 13). Additionally, the activity of $MgZnFe_2O_4$@ZSC-Cu NPs as a catalyst was compared to that of $MgZnFe_2O_4$@ZSC NPs (Entry 18). The results indicated that copper has an important role in increasing the yield of reaction.

After optimizing the reaction conditions, various aldehydes, di-aldehydes, and cyclic diketones (dimedone and cyclohexane-1,3-dione) were used in the reaction for synthesis of polyhydroquinoline (Schemes 3 and 4, Tables 2 and 3). All products were manufactured in good to high yields within short reaction times. Furthermore, the catalytic activity of $MgZnFe_2O_4$@ZSC-Cu NPs was compared with reported results in the literature (Table 4) for the model reaction. As the table shows, the synthesis of the products in the presence of catalyst, prepared from the Ziziphus spina-christi extract, is more favorable and has an acceptable efficiency compared

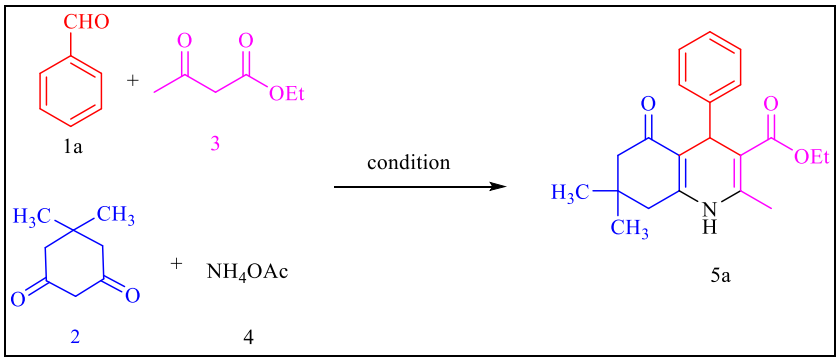

Scheme 2. Model reaction for synthesis of 5a.

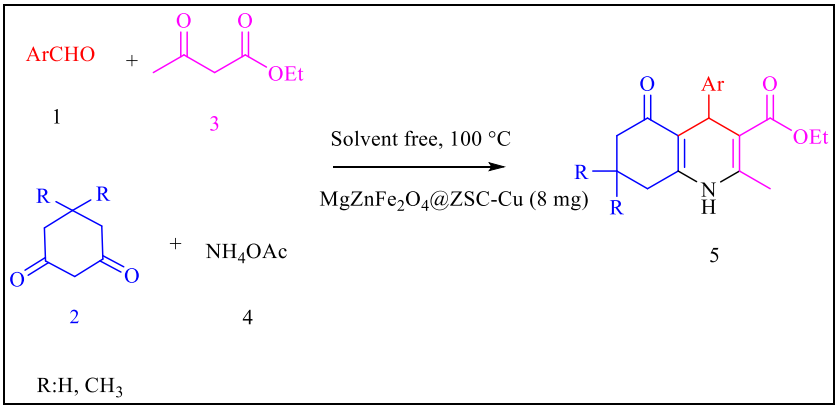

Scheme 3. $MgZnFe_2O_4$@ZSC-Cu NPs-catalyzed synthesis of mono-polyhydroquinoline derivatives.

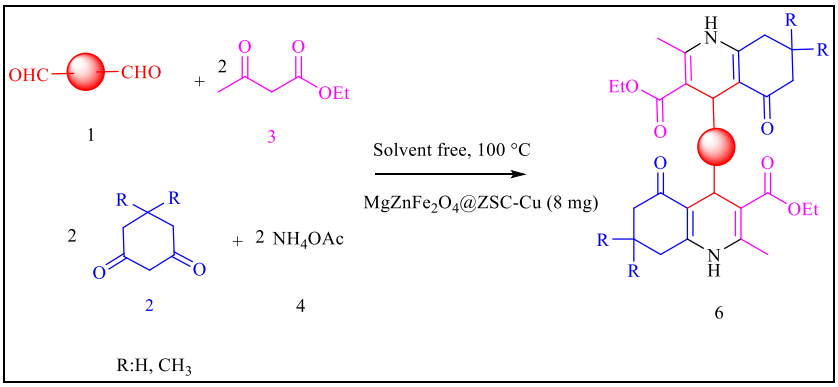

Scheme 4. $MgZnFe_2O_4$@ZSC-Cu NPs-catalyzed synthesis of bis-polyhydroquinoline derivatives.

Table 2
Synthesis of the mono-polyhydroquinoline derivatives in the presence of $MgZnFe_2O_4$@ZSC-Cu nanoparticles.

Entry	Aldehyde	Cyclic diketone	Product	Time (min)	Yield[a] (%)	M.P. (°C)		Ref.
						Found	Reported	
1	C_6H_5CHO	Dimedone	5a	4	96	204–202	203–207	[47]
2	4-FC_6H_4CHO	Dimedone	5b	10	93	198–200	180–182	[37]
3	3,4-$(OCH_3)_2$ C_6H_3CHO	Dimedone	5c	15	97	184–186	184–186	[48]
4	2,6-$(Cl)_2C_6H_3CHO$	Dimedone	5d	10	98	242–244	241–244	[37]
5	4-$NO_2C_6H_4CHO$	Cyclohexane-1,3-dione	5e	5	98	205–206	201–202	[37]
~~6~~	3-OHC_6H_4CHO	Cyclohexane-1,3-dione	5f	20	93	215–216	–	new
7	5-Br-2-OHC_6H_3CHO	Cyclohexane-1,3-dione	5g	25	95	217–220	_	new

[a] Obtaned yeild. Condition: aldehyde (1 mmol), dimedone (1 mmol, 0.14 g), ethyl acetoacetate (1 mmol, 0.13 mL), ammonium acetate (1.5 mmol, 0.12 g), $MgZnFe_2O_4$@ZSC-Cu (8 mg) under solvent free condition.

to other catalysts.

4.3. Catalyst reusability

The recoverability and stability of $MgZnFe_2O_4$@ZSC-Cu NPs were thoroughly evaluated in the production of polyhydroquinolines. A model reaction involving benzaldehyde (1) (1 mmol, 0.11 mL), dimedone (2) (1 mmol, 0.14 g), ethyl acetoacetate (3) (1 mmol, 13 mL), and ammonium acetate (4) (1.5 mmol, 0.12 g) was chosen to investigate the performance of catalyst under optimal conditions. After the reaction was completed, ethanol was added to the mixture. The catalyst was then filtered, washed with ethanol (15 mL) several times, and dried in an oven for reuse in five consecutive runs. The results, depicted in Fig. 6, displayed a slight decrease in efficiency over the runs. The structure of the reused $MgZnFe_2O_4$@ZSC-Cu as a reaction catalyst was analyzed using FT-IR (Fig. 7a), FE-SEM (Fig. 7b), and ICP-OES techniques. ICP-OES analysis of the catalyst after five successive runs revealed a Cu content of 0.78 mmol/

Table 3
Synthesis of the bis-polyhydroquinoline derivatives in the presence of $MgZnFe_2O_4$@ZSC-Cu nanoparticles.

Entry	Di-aldehyde	Cyclic diketone	Product	Time (min)	Yield[a] (%)	M.P. (°C)		Ref.
						Found	Reported	
1	2,2'-(butane-1,4-diylbis(oxy))dibenzaldehyde	Dimedone	6a	80	93	>300	_	new
2	4,4'-(butane-1,4-diylbis(oxy))dibenzaldehyde	Dimedone	6b	85	94	>300	_	new
3	4,4'-(propane-1,3-diylbis(oxy))dibenzaldehyde	Dimedone	6c	87	94	>300	_	new
4	Terephthalaldehyde	Cyclohexane-1,3-dione	6d	60	95	>300	293–294	[49]
5	4,4'-(propane-1,3-diylbis(oxy))bis(3-nitrobenzaldehyde)	Cyclohexane-1,3-dione	6e	93	98	>300	_	new

[a] Obtaned yeild. Condition: di-aldehyde (1 mmol), dimedone (2 mmol, 0.28 g), ethyl acetoacetate (2 mmol, 0.26 mL), ammonium acetate (3 mmol, 0.24 g), $MgZnFe_2O_4$@ZSC-Cu (8 mg) under solvent free condition.

Table 4
Comparison $MgZnFe_2O_4$@ZSC-Cu catalyst with other reported catalysts for synthesis of 5a.

Entry	Catalyst	Condition	Time (min)	Yield (%)	Ref.
1	MNPs-Pr-2AB@Cu	Solvent free, 100 °C	5	95	[31]
2	$CoFe_2O_4$@Pr	EtOH, reflux	400	91	[50]
3	MCM-41@PDCA-Co	Solvent free, 100 °C	10	94	[51]
4	NiFeTi $CLDH_6$	EtOH, 80 °C	6	90	[52]
5	Cu@SB-MCM-41	Solvent free, 60 °C	20 min	95	[47]
6	$MgZnFe_2O_4$@ZSC-Cu NPs	Solvent free, 100 °C	4 min	96	Present work

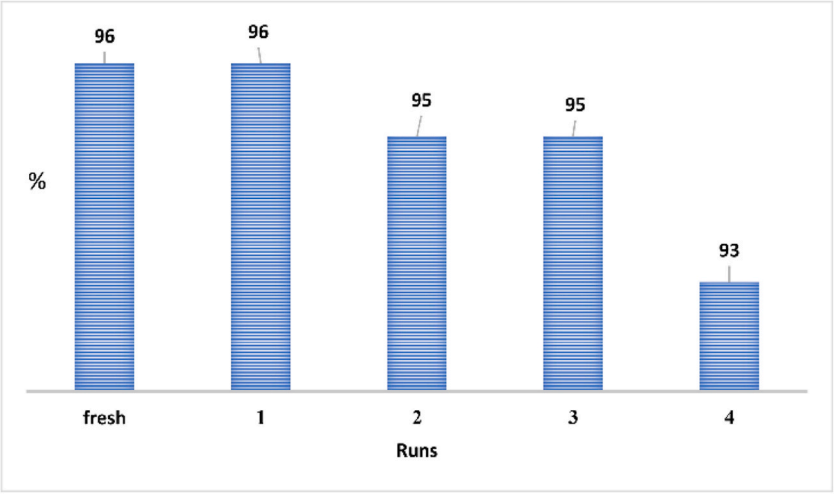

Fig. 6. Recovery of $MgZnFe_2O_4$@ZSC-Cu NPs as a catalyst in the synthesis of polyhydroquinolines.

g, closely mirroring the 0.8 mmol/g Cu loading on the fresh catalyst. These findings suggest that there were no significant alterations in the nanoparticle structure throughout the five runs.

The proposed mechanism for synthesizing polyhydroquinolines is detailed in Scheme 5. Initially, the carbonyl group of an aldehyde or ketone is activated by Cu (II) as a Lewis acid. This activation facilitates a nucleophilic attack (Knoevenagel condensation) of the enol form of β-ketone on the catalyst-activated carbonyl group, leading to the formation of intermediate (**I**). The synthesis process follows with a Michael addition of enolized ethyl acetoacetate to intermediate (**I**). This is followed by a nucleophilic attack of ammonium acetate on the carbonyl groups of intermediate (**II**), resulting in the formation of intermediate (**III**). Tautomerization then occurs, leading to the desired polyhydroquinolines as the final product [7].

5. Conclusion

As a result, copper ions were effectively loaded onto the surface of magnetic nanoparticles prepared from Ziziphus spina-christi extract, which led to the formation of [$MgZnFe_2O_4$@ZSC-Cu NPs]. These nanoparticles were thoroughly characterized using various techniques including FT-IR, SEM, TEM, XRD, TGA-DTG, and ICP-OES analyses. The environmentally friendly nature of these

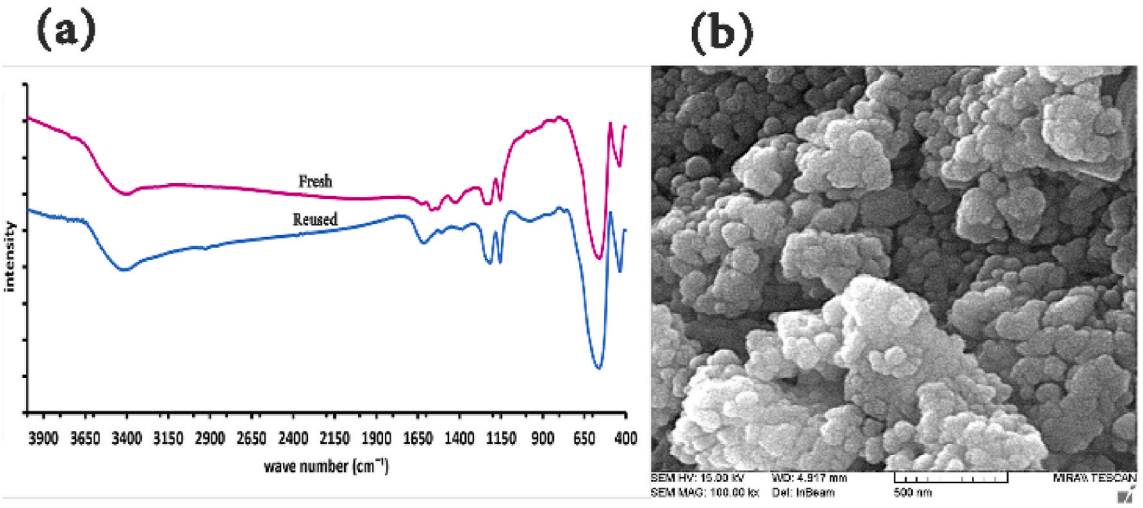

Fig. 7. FT-IR spectra of fresh and reused $MgZnFe_2O_4$@ZSC-Cu NPs as a catalyst (a), and FE-SEM image of reused catalyst (b).

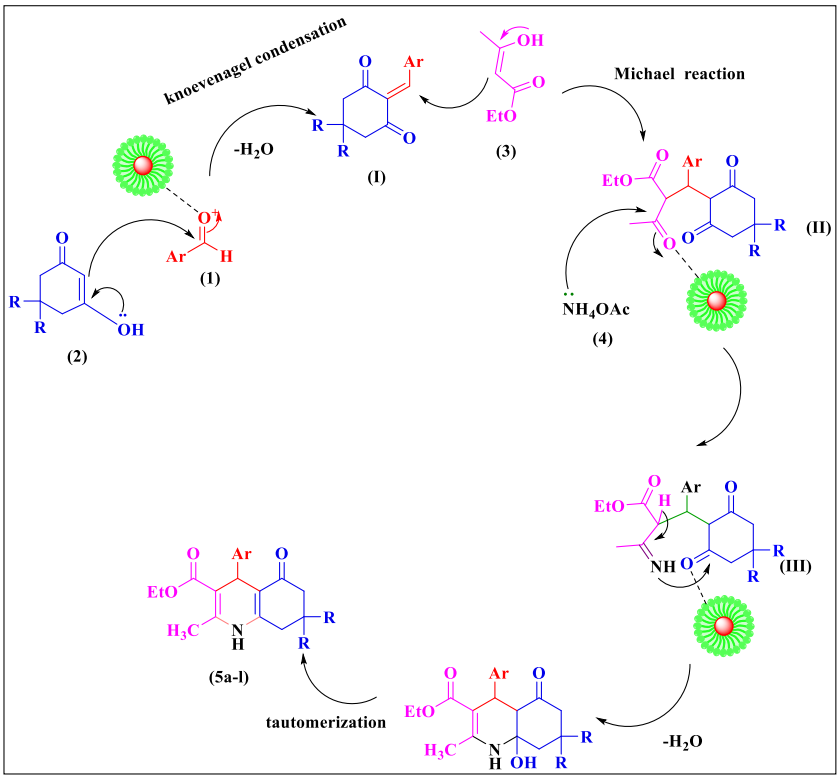

Scheme 5. A suggested mechanism for the synthesis of polyhydroquinolines in the presence of $MgZnFe_2O_4$@ZSC-Cu MNPs.

nanoparticles was highlighted by their exceptional catalytic activity in the synthesis of polyhydroquinolines. Many novel mono-, and bis-polyhydroquinolines were constructed in high yields using the Hantzsch reaction involving a four-component reaction with ethyl acetoacetate or dimedone/cyclohexane-1,3-dione, various aromatic aldehydes/di-aldehydes, and ammonium acetate. Furthermore, the catalyst demonstrated impressive reusability without significant loss of catalytic efficiency. The green catalyst offers several key advantages, including straightforward experimental procedures, short reaction times, high yields, catalyst reusability, thermal and chemical stability, solvent-free conditions, and sustainability.

Availability of data and materials

All data generated or analyzed during this study are included in this article and its supplementary information file. The spectroscopic data including FT-IR, ^{1}H NMR and ^{13}C NMR spectra of synthesized heterocyclic products are available in the supplementary material.

CRediT authorship contribution statement

Zahra Abbas-Ordoo: Writing – original draft, Software, Formal analysis. **Akbar Mobinikhaledi:** Writing – review & editing, Supervision, Project administration, Investigation, Data curation, Conceptualization. **Mohammad Ali Bodaghifard:** Writing – review & editing, Writing – original draft, Investigation.

Declaration of competing interest

The authors declare that they have no known competing financial interests or personal relationships that could have appeared to influence the work reported in this paper.

Acknowledgment

We gratefully acknowledge the financial support of this work by the research council of Arak University.

Appendix A. Supplementary data

Supplementary data to this article can be found online at https://doi.org/10.1016/j.heliyon.2024.e37151.

References

[1] T. Krasia-Christoforou, V. Socoliuc, K.D. Knudsen, E. Tombácz, R. Turcu, L. Vékás, From single-core nanoparticles in ferrofluids to multi-core magnetic nanocomposites: assembly strategies, structure, and magnetic behavior, Nanomaterials 10 (2020) 2178–2245, https://doi.org/10.3390/nano10112178.
[2] T.M. Zimina, N.O. Sitkov, K.G. Gareev, V. Fedorov, D. Grouzdev, V. Koziaeva, H. Gao, S.E. Combs, M. Shevtsov, Biosensors and drug delivery in oncotheranostics using inorganic synthetic and biogenic magnetic nanoparticles, Biosensors 12 (2022) 789–832, https://doi.org/10.3390/bios12100789.
[3] A. Mekki, M. Hachemaoui, A. Mokhtar, I. Issam, F. Bennabi, J. Iqbal, K. Rahmani, A. Bengueddach, B. Boukoussa, Catalytic behavior and antibacterial/antifungal activities of new MNPs/zeolite@ alginate composite beads, Int. J. Biol. Macromol. 198 (2022) 37–45, https://doi.org/10.1016/j.ijbiomac.2021.12.063.
[4] R.-N. Li, X.-H. Da, X. Li, Y.-S. Lu, F.-F. Gu, Y. Liu, Functionalized magnetic nanoparticles for drug delivery in tumor therapy, Chin. Phys. B 30 (2021) 017502, https://doi.org/10.1088/1674-1056/abb3e6.
[5] Y. Chen, S. Hou, Application of magnetic nanoparticles in cell therapy, Stem Cell Res. Ther. 13 (2022) 135–144, https://doi.org/10.1186/s13287-022-02808-0.
[6] Y. Lin, K. Zhang, R. Zhang, Z. She, R. Tan, Y. Fan, X. Li, Magnetic nanoparticles applied in targeted therapy and magnetic resonance imaging: crucial preparation parameters, indispensable pre-treatments, updated research advancements and future perspectives, J. Mater. Chem. B 8 (2020) 5973–5991, https://doi.org/10.1039/D0TB00552E.
[7] N. Ahadi, A. Mobinikhaledi, M.A. Bodaghifard, One-pot synthesis of 1, 4-dihydropyridines and N-arylquinolines in the presence of copper complex stabilized on MnFe2O4 (MFO) as a novel organic–inorganic hybrid material and magnetically retrievable catalyst, Appl. Organomet. Chem. 34 (2020) e5822, https://doi.org/10.1002/aoc.5822.
[8] M. Zhang, Y.-H. Liu, Z.-R. Shang, H.-C. Hu, Z.-H. Zhang, Supported molybdenum on graphene oxide/Fe3O4: an efficient, magnetically separable catalyst for one-pot construction of spiro-oxindole dihydropyridines in deep eutectic solvent under microwave irradiation, Catal. Commun. 88 (2017) 39–44, https://doi.org/10.1016/j.catcom.2016.09.028.
[9] H.-Y. Zhang, X.-P. Hao, L.-P. Mo, S.-S. Liu, W.-B. Zhang, Z.-H. Zhang, A magnetic metal–organic framework as a highly active heterogeneous catalyst for one-pot synthesis of 2-substituted alkyl and aryl (indolyl) kojic acid derivatives, New J. Chem. 41 (2017) 7108–7115, https://doi.org/10.1039/C7NJ01592E.
[10] G. Gao, J.-Q. Di, H.-Y. Zhang, L.-P. Mo, Z.-H. Zhang, A magnetic metal organic framework material as a highly efficient and recyclable catalyst for synthesis of cyclohexenone derivatives, J. Catal. 387 (2020) 39–46, https://doi.org/10.1016/j.jcat.2020.04.013.
[11] A. Ali, T. Shah, R. Ullah, P. Zhou, M. Guo, M. Ovais, Z. Tan, Y. Rui, Review on recent progress in magnetic nanoparticles: synthesis, characterization, and diverse applications, Front. Chem. 9 (2021) 629054–629079, https://doi.org/10.3389/fchem.2021.629054.
[12] W. Wu, Z. Wu, T. Yu, C. Jiang, W.-S. Kim, Recent progress on magnetic iron oxide nanoparticles: synthesis, surface functional strategies and biomedical applications, Sci. Technol. Adv. Mater. 16 (2015), https://doi.org/10.1088/1468-6996/16/2/023501, 023501-023545.
[13] A.M.E. Shafey, Green synthesis of metal and metal oxide nanoparticles from plant leaf extracts and their applications: a review, Green Process. Synth. 9 (2020) 304–339, https://doi.org/10.1515/gps-2020-0031.
[14] B. Mahesh, A comprehensive review on current trends in greener and sustainable synthesis of ferrite nanoparticles and their promising applications, Results Eng (2023) 101702, https://doi.org/10.1016/j.rineng.2023.101702.
[15] A. Rohaizad, S. Shahabuddin, M.M. Shahid, N.M. Rashid, Z.A.M. Hir, M.M. Ramly, K. Awang, C.W. Siong, Z. Aspanut, Green synthesis of silver nanoparticles from Catharanthus roseus dried bark extract deposited on graphene oxide for effective adsorption of methylene blue dye, J. Environ. Chem. Eng. 8 (2020) 103955–103965, https://doi.org/10.1016/j.jece.2020.103955.
[16] P.E. Das, I.A. Abu-Yousef, A.F. Majdalawieh, S. Narasimhan, P. Poltronieri, Green synthesis of encapsulated copper nanoparticles using a hydroalcoholic extract of Moringa oleifera leaves and assessment of their antioxidant and antimicrobial activities, Molecules 25 (2020) 555–572, https://doi.org/10.3390/molecules25030555.
[17] A.K. Mittal, Y. Chisti, U.C. Banerjee, Synthesis of metallic nanoparticles using plant extracts, Biotechnol. Adv. 31 (2013) 346–356, https://doi.org/10.1016/j.biotechadv.2013.01.003.
[18] J. Asgarpanah, E. Haghighat, Phytochemistry and pharmacologic properties of Ziziphus spina christi (L.) Willd, Afr. J. Pharm. Pharmacol. 6 (2012) 2332–2339, https://doi.org/10.5897/AJPP12.509.

[19] B.H. Shnawa, P.J. Jalil, S.M. Hamad, M.H. Ahmed, Antioxidant, protoscolicidal, hemocompatibility, and antibacterial activity of nickel oxide nanoparticles synthesized by Ziziphus spina-christi, Bionanoscience 12 (2022) 1264–1278, https://doi.org/10.1007/s12668-022-01028-3.
[20] H.M. Adamu, O. Abayeh, N. Ibok, S.E. Kafu, Antifungal activity of extracts of some Cassia, Detarium and Ziziphus species against dermatophytes, NIScPR. 5 (2006) 357–360. http://nopr.niscpr.res.in/handle/123456789/8004.
[21] M.-N. Chen, L.-P. Mo, Z.-S. Cui, Z.-H. Zhang, Magnetic nanocatalysts: synthesis and application in multicomponent reactions, Curr. Opin. Green Sustainable Chem. 15 (2019) 27–37, https://doi.org/10.1016/j.cogsc.2018.08.009.
[22] D. Zeleke, T. Damena, Advance in green synthesis of pharmacological important heterocycles using multicomponent reactions and magnetic nanocatalysts (MNCs), Results Chem 7 (2023) 101283–101302, https://doi.org/10.1016/j.rechem.2023.101283.
[23] N. Ahadi, A. Mobinikhaledi, A.H. Ebrahimi, Zn complexed on hybrid manganese doped cobalt ferrite nanoparticles covered by silica as a catalyst in the synthesis of 2-amino-4H-pyran and N-arylquinoline derivatives, Heliyon 10 (2024) e30620, https://doi.org/10.1016/j.heliyon.2024.e30620.
[24] I.V. Machado, J.R. Dos Santos, M.A. Januario, A.G. Corrêa, Greener organic synthetic methods: sonochemistry and heterogeneous catalysis promoted multicomponent reactions, Ultrason. Sonochem. 78 (2021) 105704–105795, https://doi.org/10.1016/j.ultsonch.2021.105704.
[25] N. Ahadi, A. Mobinikhaledi, A. Fathehesami, Z. Bagheri, Zn salen complex supported on MnCoFe2O4 (MCF) magnetic nanoparticles as a catalyst in the synthesis of 3, 4-dihydropyrimidin-2 (1H)-ones/thiones (Biginelli-like reaction), Res. Chem. Intermed. 48 (2022) 2469–2488, https://doi.org/10.1007/s11164-022-04709-6.
[26] Yu H. Zainab, N.U. Rehman, M. Ali, A. Alam, A. Latif, N. Shahab, I. Amir Khan, A. Jabbar Shah, M. Khan, Novel polyhydroquinoline-hydrazide-linked Schiff`s base derivatives: multistep synthesis, antimicrobial, and calcium-channel-blocking activities, Antibiotics 11 (2022) 1568–1587, https://doi.org/10.3390/antibiotics11111568.
[27] X.-H. Yang, P.-H. Zhang, Y.-H. Zhou, C.-G. Liu, X.-Y. Lin, J.-F. Cui, Synthesis and antioxidant evaluation of novel 4-aryl-hexahydroquinolines from lignin, ARKIVOC (Gainesville, FL, U. S.) 10 (2011) 327–337, https://doi.org/10.3998/ark.5550190.0012.a27.
[28] R. Surasani, D. Kalita, A.D. Rao, K. Yarbagi, K. Chandrasekhar, FeF3 as a novel catalyst for the synthesis of polyhydroquinoline derivatives via unsymmetrical Hantzsch reaction, J. Fluor. Chem. 135 (2012) 91–96, https://doi.org/10.1016/j.jfluchem.2011.09.005.
[29] S.T. Fardood, A. Ramazani, S. Moradi, Green synthesis of Ni–Cu–Mg ferrite nanoparticles using tragacanth gum and their use as an efficient catalyst for the synthesis of polyhydroquinoline derivatives, J. Sol. Gel Sci. Technol. 82 (2017) 432–439, https://doi.org/10.1007/s10971-017-4310-6.
[30] B. Maleki, O. Reiser, E. Esmaeilnezhad, H.J. Choi, SO3H-dendrimer functionalized magnetic nanoparticles (Fe3O4@ DNH (CH2) 4SO3H): synthesis, characterization and its application as a novel and heterogeneous catalyst for the one-pot synthesis of polyfunctionalized pyrans and polyhydroquinolines, Polyhedron 162 (2019) 129–141, https://doi.org/10.1016/j.poly.2019.01.055.
[31] Mohammadizadeh Z. Najahi, M. Hamidinasab, N. Ahadi, M.A. Bodaghifard, A novel hybrid organic-inorganic nanomaterial: preparation, characterization and application in synthesis of diverse heterocycles, Polycycl. Aromat. Comp. 42 (2022) 1282–1301, https://doi.org/10.1080/10406638.2020.1776346.
[32] N. Ahadi, A. Mobinikhaledi, R.M. Hosseini, An application study of MnCoFe2O4@ PEG-4000 (MCF@ PEG-4000) MNPs as a catalyst in the synthesis of hexahydroquinolines and benzopyrans and as an nano-adsorbent for the removal of Cu (II) and Fe (III) ions in aqueous solutions, J. Nanoparticle Res. 25 (2023) 46–61, https://doi.org/10.1007/s11051-023-05689-3.
[33] A. Mobinikhaledi, N. Foroughifar, M.A.B. Fard, H. Moghanian, S. Ebrahimi, M. Kalhor, Efficient one-pot synthesis of polyhydroquinoline derivatives using silica sulfuric acid as a heterogeneous and reusable catalyst under conventional heating and energy-saving microwave irradiation, Synth. Commun. 39 (2009) 1166–1174, https://doi.org/10.1080/00397910802513060.
[34] Y. Sun, Y. Zhang, W. Qi, J. Xie, X. Cui, Saponins extracted by ultrasound from Zizyphus jujuba Mil var. spinosa leaves exert resistance to oxidative damage in Caenorhabditis elegans, J. Food Meas. Char. 15 (2021) 541–554, https://doi.org/10.1007/s11694-020-00653-4.
[35] H. Bayahia, The highly efficient green synthesis of nanostructured ZnFe2O4 photocatalysts by using Ziziphus mauritiana and Salvadora persica extracts for the photocatalytic degradation of crystal violet in sunlight, J. King Saud Univ. Sci. 35 (2023) 102584–102594, https://doi.org/10.1016/j.jksus.2023.102584.
[36] Z. Kordrostami, Design, characterization and application of SO3H-functionalized phthalimide as a highly efficient catalyst for the condensation of dimedone with arylaldehydes, β-ketoesters and ammonium acetate, Org. Chem. Res. 2 (2016) 197–207, https://doi.org/10.22036/ORG.CHEM..2016.17602.
[37] D. Khan, Shaily, N. Maurya, Microwave-assisted IBX-mediated one-pot four-component synthesis of 4-arylhexahydroquinoline derivatives from benzyl alcohols: a metal-free approach, Russ. J. Org. Chem. 59 (2023) 695–703, https://doi.org/10.1134/S107042802304019X.
[38] S. Tasqeeruddin, Y. Asiri, S. Shaheen, Zirconium (IV) oxychloride octahydrate (ZrOCl2· 8H2O): an efficient catalyst for the one-pot multicomponent synthesis of hexahydroquinoline derivatives under conventional heating and microwave irradiation, Russ. J. Org. Chem. 58 (2022) 1008–1014, https://doi.org/10.1134/S1070428022070107.
[39] S. Yallappa, J. Manjanna, B. Dhananjaya, U. Vishwanatha, B. Ravishankar, H. Gururaj, Phytosynthesis of gold nanoparticles using Mappia foetida leaves extract and their conjugation with folic acid for delivery of doxorubicin to cancer cells, J. Mater. Sci. Mater. Med. 26 (2015) 1–12, https://doi.org/10.1007/s10856-015-5567-3.
[40] T. Tatarchuk, M. Myslin, I. Mironyuk, M. Bououdina, A.T. Pędziwiatr, R. Gargula, B.F. Bogacz, P. Kurzydło, Synthesis, morphology, crystallite size and adsorption properties of nanostructured Mg–Zn ferrites with enhanced porous structure, J. Alloys Compd. 819 (2020) 152945–152960, https://doi.org/10.1016/j.jallcom.2019.152945.
[41] T. Tatarchuk, A. Shyichuk, N. Danyliuk, M. Naushad, V. Kotsyubynsky, V. Boychuk, Cobalt ferrite as an electromagnetically boosted metal oxide hetero-Fenton catalyst for water treatment, Chemosphere 326 (2023) 138364–138375, https://doi.org/10.1016/j.chemosphere.2023.138364.
[42] I. Starko, T. Tatarchuk, M. Naushad, N. Danyliuk, Enhanced activity of La-substituted nickel–cobalt ferrites in Congo red dye removal and hydrogen peroxide decomposition, Water, Air, Soil Pollut. 235 (2024) 527–535, https://doi.org/10.1007/s11270-024-07329-5.
[43] H. Liu, A. Li, X. Ding, F. Yang, K. Sun, Magnetic induction heating properties of Mg1-xZnxFe2O4 ferrites synthesized by co-precipitation method, Solid State Sci. 93 (2019) 101–108, https://doi.org/10.1016/j.solidstatesciences.2019.05.005.
[44] A. Mishra, M. Soni, Synthesis, structural, and biological studies of some Schiff bases and their metal complexes, Met.-Based Drugs. 2008 (2008) 1–7, https://doi.org/10.1155/2008/875410.
[45] R. Bosigo, L.M. Lepodise, A. Kuvarega, C. Muiva, Hydrothermal synthesis of CuO and CeO2/CuO nanostructures: spectroscopic and temperature dependent electrical properties, J. Mater. Sci. Mater. Electron. 32 (2021) 7136–7152, https://doi.org/10.1007/s10854-021-05423-6.
[46] K. Petcharoen, A. Sirivat, Synthesis and characterization of magnetite nanoparticles via the chemical co-precipitation method, Mater. Sci. Eng. B 177 (2012) 421–427, https://doi.org/10.1016/j.mseb.2012.01.003.
[47] M. Shaker, A.S. Beni, Cu@ SB-MCM-41 composite as an efficient and recyclable nanocatalyst for the synthesis of polyhydroquinoline derivatives via unsymmetrical Hantzsch reaction, J. Porous Mater. 28 (2021) 435–449, https://doi.org/10.1007/s10934-020-01006-8.
[48] S. Mule, D. Pansare, V. Gore, A facile, one-pot synthesis of 1, 4-dihydropyridine derivative by using polyaniline supported zinc oxide nanoparticle via Hantzsch reaction, Lett. Appl. NanoBioSci. 12 (2023) 17–31, https://doi.org/10.33263/LIANBS121.017.
[49] O. Goli-Jolodar, F. Shirini, M. Seddighi, Introduction of a novel nanosized N-sulfonated Brönsted acidic catalyst for the promotion of the synthesis of polyhydroquinoline derivatives via Hantzsch condensation under solvent-free conditions, RSC Adv. 6 (2016) 26026–26037.
[50] T. Tamoradi, S.M. Mousavi, M. Mohammadi, Praseodymium (iii) anchored on CoFe 2 O 4 MNPs: an efficient heterogeneous magnetic nanocatalyst for one-pot, multi-component domino synthesis of polyhydroquinoline and 2, 3-dihydroquinazolin-4 (1 H)-one derivatives, New J. Chem. 44 (2020) 3012–3020, https://doi.org/10.1039/C9NJ05468E.
[51] S. Sharma, U.P. Singh, A. Singh, Synthesis of MCM-41 supported cobalt (II) complex for the formation of polyhydroquinoline derivatives, Polyhedron 199 (2021) 115102–115113, https://doi.org/10.1016/j.poly.2021.115102.
[52] G. Rathee, S. Kohli, N. Singh, A. Awasthi, R. Chandra, Calcined layered double hydroxides: catalysts for xanthene, 1, 4-dihydropyridine, and polyhydroquinoline derivative synthesis, ACS Omega 5 (2020) 15673–15680, https://doi.org/10.1021/acsomega.0c01901.